A METHOD TO DEFINE A SCALABLE TURBULENCE RESPONSE MODEL FOR THE SHIP-HELICOPTER DYNAMIC INTERFACE

Thomas R. Fell, Michael Jump (mjump1@liverpool.ac.uk), Mark D. White and Ieuan Owen
University of Liverpool, UK

and

Bryan Finlay
Dstl, UK

Abstract

Maritime helicopters are often required to operate in the turbulent flow or air wake generated in the lee of a ship's superstructure. This turbulent air wake disturbs the aircraft motion and therefore compensatory control inputs need to either be provided by a pilot or a control system for accurate station keeping. This paper presents the method used to understand how aircraft size, expressed as either maximum take-off weight or rotor disc loading, affects the turbulent response of an aircraft operating in a ship's air wake. Details of the simulation implementation and investigation are given. The turbulence responses of the aircraft are analyzed using frequency domain system identification techniques and low order equivalent systems are identified. The results of this analysis were then captured using a simple scaling law to provide an approximation of an aircraft's turbulence response using the ambient wind-speed and aircraft disc loading. The derived scalable turbulence model consists of a transfer function whose standard deviation and break frequency relate to the ambient wind velocity and the rotor disc loading. 'Conservative', 'Standard' and 'Optimistic' versions of the model were created. For the standard deviation model parameter, the 'Standard' version of the model appears to be the best fit, except for the pitch and roll axes of stiffer hingeless or teetering rotor head vehicles, where the 'Conservative' fit appears to be the better model. The 'Standard' model appears to be the best fit for all rotorcraft types for the break frequency parameter of the model.

1. INTRODUCTION

Rotorcraft are in routine use throughout the world's navies. They provide a powerful and flexible means to conduct tasks and operations that would be otherwise difficult or impossible from a fixed operating base by operating from ships far from land. These tasks include but are not limited to: anti-submarine and anti-surface unit warfare, troop transfers and re-supply tasks including the delivery of humanitarian aid to natural disaster areas. It is acknowledged that the operation of a helicopter in the immediate locality of the ship is one of the most difficult tasks that a pilot can be asked to perform, particularly in adverse weather conditions. The motion of the ship, as well as the dynamic air wake that results from airflow over the ship's super-structure, all contribute to a challenging flying environment – the ship dynamic interface (DI).

In order for a helicopter-ship combination to become operational, it is usual for test crews to perform numerous launch and recovery tasks to the ship whilst at sea to establish the safe limits of performance, handling and structural loads. Tests will be carried out for a number of different wind strengths and directions relative to the ship's heading and will cater for the range of aircraft operating masses and configurations. This work verifies that the design of the aircraft (or the ship) is suitable and safe and generates data which enables the Ship-Helicopter Operating Limits (SHOL) to be ascertained. An example of the tools and techniques used for this are provided in Ref. [1].

In recent times, significant research effort has been expended on understanding the ship DI and the pilot/vehicle role within it. This research has included studies that have used real ships and helicopters e.g. Ref. [2], but, has also focused on the potential increased role of modelling and simulation. These provide a means to improve the process of deriving SHOLs by reducing cost, the time taken and the risk associated with their generation for a given helicopter-ship combination [3, 4]. Research has been conducted to develop computational techniques for generating air wakes around a given ship geometry [5, 6] and for assessing their impact on pilot workload in piloted simulation trials [5, 7]. As

well as supporting test and evaluation to derive SHOLs, the research has provided insight into the nature of the complex unsteady shear layers and vortical flow features around ships, and the impact of this turbulence on helicopter control.

At the same time as research has been developing the state of the art in terms of modelling SHOLs for manned helicopters, rotary wing (RW) unmanned aerial systems (UAS) have begun to operate from ships. Many of these RW UAS are much smaller than manned helicopters. For example, the Schiebel CAMCOPTER® UAV, has a maximum take-off mass of 200kg. Given their size and the absence of a human pilot, the impact of the air wake in the lee of the ship's superstructure on UAS is likely to be a different to that of manned helicopters. The magnitude, frequency content and dimensions of the flow features are all expected to have a significant effect on the dynamics and control margins of the UAS control system architecture.

From the perspective of a procurement authority, it is important to be able to specify the design and acceptance requirements for any system. With the emergence of RW UAS that are intended to operate from ships, there is a gap in the design criteria which underpin safe and effective operational capability. The determination of Flying Qualities Requirements (FQRs) for maritime UAS is therefore important for future procurement of UAS intended to operate in this environment.

The current literature on Maritime UAS research is predominantly focused on the recovery methods for, and equipment used, in ship-borne operations. A variety of methods are being explored including Ship Relative GPS (SRGPS), millimetre-wave radar (Ref. 2), Laser Rangefinder (Ref. 3), Optical (Ref. 4) and ship motion prediction (Ref. 5). The paper that reports upon the ongoing performance optimization work on the MQ-8 (Fire Scout) by Ferrier et al. (Ref. 2) presents a successful implementation of an Energy Index (EI) system applied to the DI between aircraft and ship. The EI system provides a means of quantifying the acceptable limits for ship motion and aircraft structural limits.

Whilst much of this literature focuses on solving the recovery problem in practical hardware terms, the research reported in this paper takes a different approach. It uses the tools, techniques and experience gathered in modelling and simulating manned rotorcraft in the ship's DI at the University of Liverpool (UoL). This work has been primarily focused on the reduction of cost and risk of aircraft-ship operation qualification through the use of human-in-the-loop flight simulation.

The issue here is that UAS can come in a far wider range of shapes and sizes than their manned counterparts. In order to tackle this problem, a number of discrete steps had to be performed. The first of these was to develop a method that would allow a scalable turbulence response model of the ship dynamic interface to be created. The second step was to exercise this model with a variety of helicopter dynamic response parameters to allow predictions to be made as to what characteristics would be, or would not be, favorable for a given platform operating in the air wake of a ship (or, indeed, any turbulent environment). This paper reports upon the first of these tasks.

Section 2 describes the process used to create what is being called a 'Scalable Turbulence Model' (STM) and Section 3 presents the STM itself. Section 4 discusses the results achieved and the paper is concluded in Section 5.

2. PROCESS TO CREATE THE SCALABLE TURBULENCE MODEL

2.1. Overview

Figure 1 shows the steps that are required to generate the scalable turbulence response model.

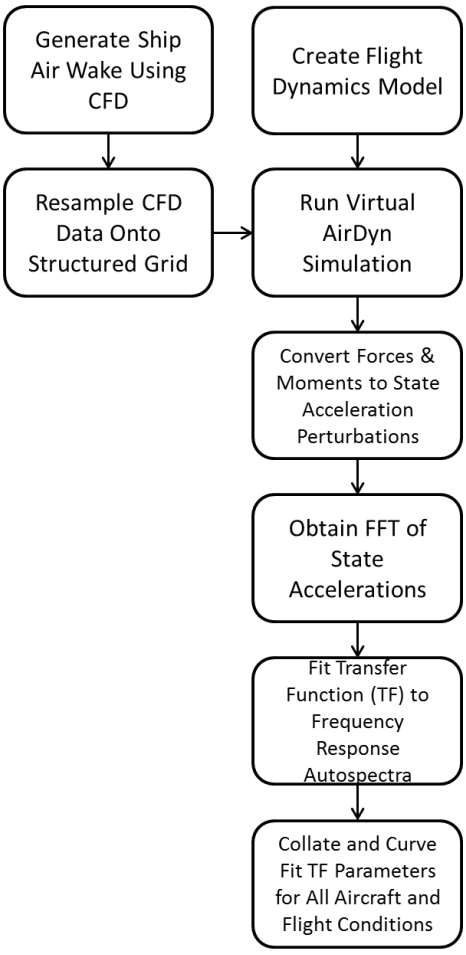

Figure 1. Flow chart indicating the process followed to derive the Scalable Turbulence Model

A computational fluid dynamics (CFD) code is employed to generate a representative air wake around a known ship configuration. At the same time, a flight dynamics model (FDM) of the helicopter under consideration must also be created. Once these two components have been generated, the FDM is trimmed at the required ambient atmospheric conditions and then fixed in position in the wake. The resultant forces and moments that result from the wake flow perturbations can then be recorded.

The following Sections provide more detail and sample results from each of the steps involved.

2.1.1. Flight Dynamics Models

In order to conduct the study and to capture the impact of rotorcraft size, six rotorcraft flight dynamics models were used. They were all developed in FLIGHTLAB, a multi-body simulation environment made up of predefined system component models. The five rotorcraft models were based upon: (i) Sikorsky Seahawk SH-60B; (ii) Bell 412HP; (iii) Airbus Helicopters BO-105; (iv) Northrop Grumman Firescout MQ-8B; (v) Yamaha R-MAX and the (vi) Align T-Rex 700. Each helicopter model makes use of a blade-element main rotor with a Peters-He inflow model, a Bailey rotor for the tail rotor, and fuselage and empennage aerodynamic look-up tables. The RMAX and T-Rex models in addition have stability bars which are modelled as rate feedback gain in the roll and pitch channels.

In order for a FLIGHTLAB model to interact with an air wake in a simulation environment, the structured unsteady air wake velocities are able to interact with the model using built-in air load computation points (ACPs), distributed around the helicopter model. These velocities are used to compute the aerodynamic forces and moments in all three axes that act at or around the helicopter model centre of gravity (c.g.).

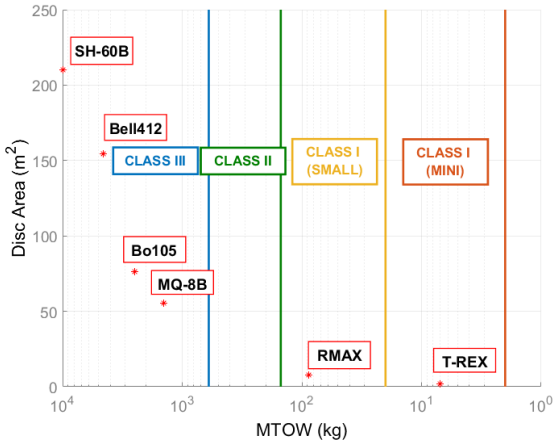

Figure 2. Flight Dynamics Models Selected for the Study

The range of selected rotorcraft models was based partly upon the NATO UAS classification system [12] and partly because they were rotorcraft models that were readily available at UoL. The system broadly divides rotorcraft into three classes by Maximum Take-Off Weight (MTOW) and further subdivides by operating limits and aircraft role. The aircraft selected for this research are presented in Figure 2 as a function of rotor disc area and MTOW. The NATO UAS classification boundaries are also marked for each class investigated. The models used provide a reasonable spread across the various classes in terms of both rotor disc area and MTOW. The SH60B, MQ8B, RMAX and TREX rotorcraft models were used to derive an initial version of the scalable turbulence model. The B412HP and BO10 rotorcraft models were used as validation cases for this turbulence model.

2.1.2. Ship Air Wake Generation

The ship air wake model makes use of a time-accurate CFD technique, Detached Eddy Simulation (DES). The high fidelity CFD air wake solutions are performed using ANSYS Fluent software, employing the Delayed Detached Eddy Simulation (DDES) SST k-ω based turbulence model with third-order accuracy [13].

The time-accurate unsteady unstructured CFD simulations contain three air wake velocity components in the three-dimensional spatial domain. In the original operation of the process, the unstructured CFD solution is computed for 45 seconds at 100Hz for a domain/volume with radius of four times the length of the ship, L. The first 15 seconds of the data are discarded to allow the unsteady solution to settle, giving 30 seconds of useable flow solution. The solution domain is illustrated in Figure 3 with a more detailed vertical plane closer-in to the area of interest for this study (the ship's flight deck) shown in Figure 4.

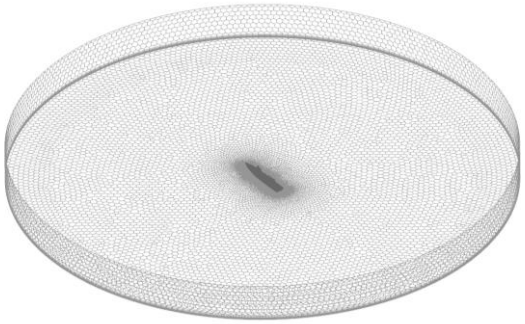

Figure 3. Unstructured CFD mesh domain

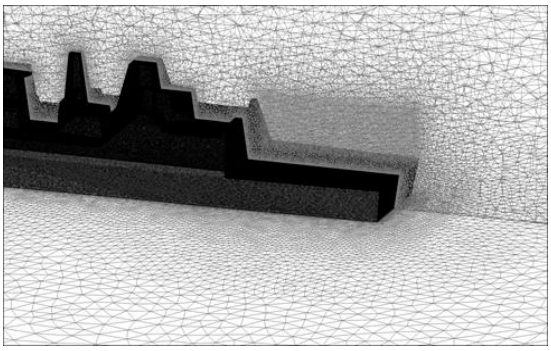

Figure 4. Two-dimensional plane showing unstructured CFD mesh

For the results presented in this paper, the air wake was generated using the geometry representative of a UK Type 45 Destroyer. This approach has been previously validated against experimental data as described in Ref. [13] and was applied in this research to ensure accurate capture of the unsteady flow conditions.

2.1.3. Resampled Data on Structured Grid

One of the end goals of the research was to be able to demonstrate the efficacy of the methods developed using real-time simulation. In order to be able to use the FLIGHTLAB real-time simulation environment, the unstructured CFD solution data had to be sampled and interpolated onto a smaller structured grid [14]. In the normal operation of this process, the grid spacing used for the structured grid is 1m in all three orthogonal axes. To avoid generating large datasets, the CFD data is also down-sampled to 25Hz and is confined to a domain-of interest aft of the ship's hangar door. Figure 5 shows the overall dimensions of the structured grid used in the work and Figure 6 shows an example of the instantaneous vertical velocity perturbation in the computed flow field after it has been sampled onto the structured grid. The example data is taken from a horizontal slice 7m above deck, 15 seconds into the final flow solution for a nominal wind speed of 40kts with the wind coming from the starboard side at 45 degrees to the deck orientation (known as 'Green 45'). The extent of the ships' deck is represented by the dotted line.

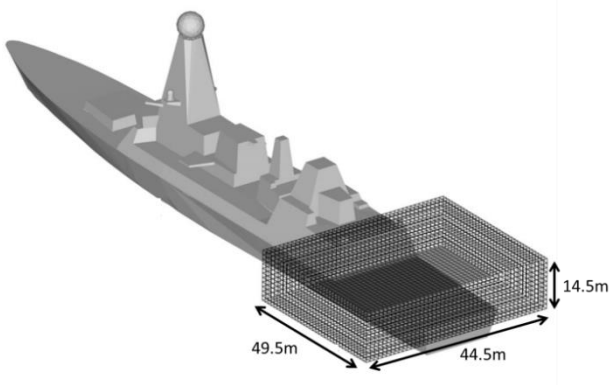

Figure 5. Structured grid used for Virtual AirDyn process

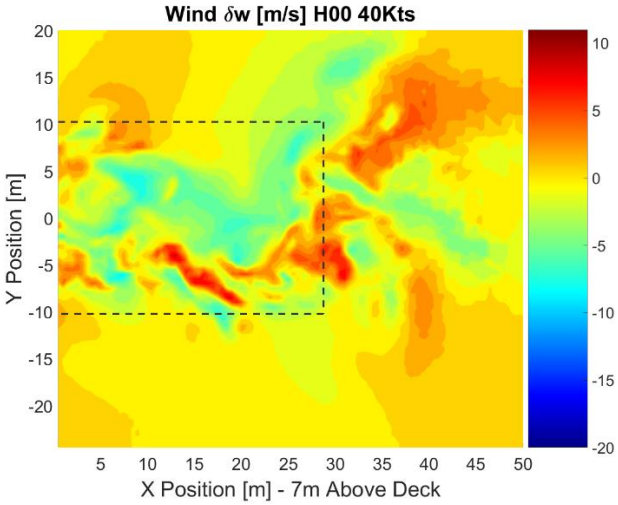

Figure 6. Example instantaneous vertical velocity perturbation, 'w', for a 40kt Headwind for time = 15s

2.1.4. Virtual AirDyn

The Virtual AirDyn (VAD) [15] is a software-based version of an experimental AirDyn, developed and used at UoL, where an instrumented rotorcraft model with a motorized rotor can be placed in the wake of a model ship and the loads imparted to the rotorcraft in the wake measured. In the VAD, the wake is generated using the CFD techniques described previously and the physical rotorcraft model is replaced by a FLIGHTLAB flight dynamics model. The technique resolves the unsteady aerodynamic forces and moments generated by the ship air wake on the rotorcraft by fixing the flight dynamics model at various specified points around the ship's deck, within the structured grid box shown in Figure 5. The simulation is then run with the rotorcraft fixed in place but with the rotor free to rotate, flap, and lead-lag (where applicable) under power with the governor engaged to maintain constant rotor RPM. In this way, the unsteady forces and moments that would act on the vehicle can be measured.

Figure 7 shows the grid of points used to sample these forces and moments on the rotorcraft models used for the study. The cross symbol indicates the location of the aircraft c.g. position when perturbation data is sampled; the numbers indicate the sequence of sampling points used; the dashed line indicates the extent of the structured grid of data points and the solid lines indicate the extent either of the ship's deck or the rotor disk for the SH-60 helicopter model. Each grid point is uniformly spaced in each direction at 11.5ft. This spacing and distribution provided a compromise between ensuring that the largest rotocraft model's rotor remained inside the air wake grid box at all times (as shown in the Figure), good

coverage of the air wake for the smaller rotorcraft models, the size of the resulting data files produced and the time taken to produce them by the VAD process.

Figure 7. Perturbation data sampling points within the

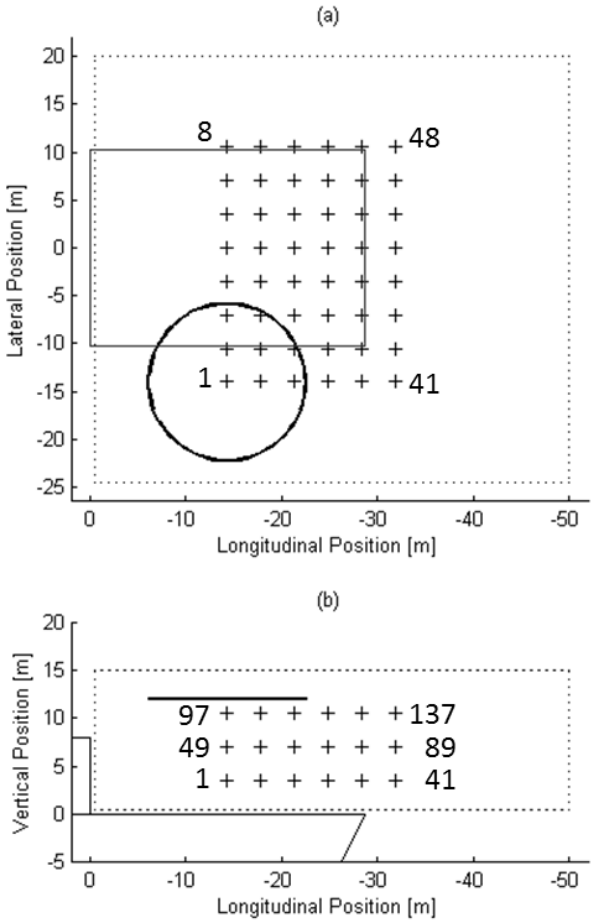

structured grid airwake

2.1.5. Conversion of Forces and Moments to State Accelerations

The outputs from the VAD process are the total summed forces and moments acting at the aircraft's c.g. The time history record signals are then converted into accelerative state perturbations by first subtracting the mean of each signal and then dividing by the aircraft's mass or inertia tensor for translational and rotational motion respectively.

2.1.6. Obtain FFT of State Accelerations

The next stage of the process is to pass the state accelerations through the multi-window frequency response identification routine used by CIFER® [16] which analyses the signal with a range of window sizes to maximize the accuracy of the identified response across the frequency range of interest. For manned flight dynamics, this range is traditionally between 1-10 rad/s. However, due to the large range of aircraft sizes under investigation, this range was extended upwards to 40 rad/s to accommodate the small UAS models whose turbulence cut-off frequencies were generally found to be much higher than the larger manned helicopters. The value selected is greater than twice the highest cut-off frequency to ensure that the identified response was not artificially skewed by using a more limited frequency range.

The lower frequency range is limited by the total signal length used in the identification. In CIFER, this is based on there being at least two full oscillations present in the largest window size used. All aircraft responses were processed using the lowest possible identifiable frequency up to 40rad/s, as the higher frequency information was found to have a negligible effect on the results produced for the larger aircraft.

2.1.7. Fit Transfer Function to Obtain a Non-Parametric Response Autospectra

The output of this CIFER system identification is the non-parametric turbulence frequency response autospectra for each translational and rotational axis for each helicopter. The autospectra are then approximated by a parametric 2nd order transfer function (Eq. 1) which was found to have the closest least-squares fit to the non-parametric response. This simple form was chosen to more easily facilitate the development of a scaling law based on the scaling of just two parameters: the turbulence corner frequency, ω, and the magnitude variance or turbulence intensity, σ. This rational transfer function can be driven by a Gaussian white noise signal with unit variance to yield an output with the same spectral properties as the original time history.

$$G_a(s) = \frac{\sigma\omega^2}{(s+\omega)^2} \quad (1)$$

An acceptable fit was achieved for all aircraft by limiting the fit to the frequency range that contained the majority of the turbulent energy. The upper frequency limit of the fit was set by calculating the frequency at 95% of the cumulative RMS of the relevant translational or rotational perturbation accelerations with the remaining frequency response information discounted. The cost function of Eq. 2 used is a reduced version of the function used in CIFER where a linear spread of points are evaluated between the lower and upper frequency limits.

$$J = \frac{20}{n_\omega}\sum_{\omega_1}^{\omega_{n_\omega}}\left(\left|\hat{T}_c\right| - |T|\right)^2 \quad (2)$$

A cost between 50 and 100 is deemed an acceptable fit, whilst less than 50 is considered almost indistinguishable from the original signal [16].

Figure 8 provides an illustrative example of a transfer function alongside the cumulative RMS with the 95% frequency marked.

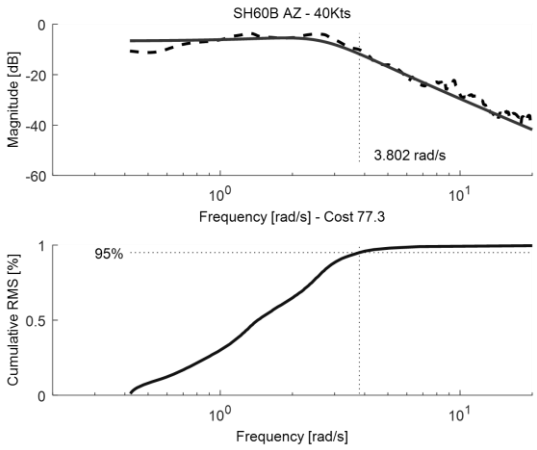

Figure 8. Transfer function fit and cumulative RMS for SH-60B helicopter in a 40kt headwind

2.1.8. Collate and Curve Fit Transfer Function Data for all Aircraft and Flight Conditions

The final goal of this process is to define a set of transfer functions to describe the turbulent response of an aircraft with a given disc loading. To do this, it is necessary to establish describing parameters for sigma (magnitude variance) and omega (break frequency) terms in Eq. 1 based upon the parameters that have been varied. Specifically, the ambient freestream wind speed and the disc loading representing the variation in aircraft size. Equations 3 and 4 show the form of the curves to which the data has been fitted with the coefficients a, b and c being found using a least squares regression fitting process.

(3) $$\sigma = a_\sigma U^{b_\sigma} \left(\frac{M}{\pi R^2}\right)^{c_\sigma}$$

(4) $$\omega = a_\omega U^{b_\omega} \left(\frac{M}{\pi R^2}\right)^{c_\omega}$$

3. THE SCALABLE TURBULENCE MODEL - RESULTS

Prior to the generation of the results to be presented in what follows, a sensitivity study was conducted into a number of the parameters used for the investigation. Space constraints preclude the inclusion of the full results from this study but the parameters used to generate the results presented in this paper are:

a. a CFD re-sampling structured grid spacing of 0.5m;
b. a CFD re-sampling frequency of 100Hz and
c. a repeating air wake time history of 90s.

The remainder of this Section presents some typical results generated by the process described in Section 2, using the recommended parameters listed above, to generate a scalable turbulence model (STM). In the interests of clarity and conciseness, not all results are presented here. The results for the STM are presented in three sections. The first show the results for the initial STM generated using the four initial helicopter models (UH-60B, MQ-8B, RMAX and TREX). The second set of results show how the 'unseen' helicopter models (Bell 412HP, BO105) compare to this STM. The final set of results shows an updated scalable turbulence model based upon all six helicopter models used.

3.1 Four Aircraft-based STM

Figure 9(a) shows the σ values obtained for the initial four test aircraft and the corresponding fit obtained for each of the four wind speeds as a function of disk loading for the translational heave axis. The fit was achieved by the algorithm considering all data points being weighted equally. Figure 9(b) shows the ω values obtained for the same axis.

Figure 10 shows the corresponding σ and ω for the rotational pitch axis. The applicable coefficients used to generate the curves from Eqns. 3 and 4 are given in the Appendix.

3.2 Unseen Aircraft Comparison with the Four Aircraft-based STM

The power of any model lies in its ability to accurately predict the outcome of the process it is designed to describe. As such, the two 'unseen' aircraft (Bell 412HP and BO105) were also put through the process of Figure 1 and the results compared with the STM curve fits presented in the previous Section. Figure 11 and Figure 12 show the results of this exercise, again for the translational heave and rotational pitch axes respectively.

3.3 Six Aircraft-based STM

With a total of six aircraft analyzed it was considered a sensible course of action to re-fit the STM curves to all of the data. In addition, given the observations regarding the quality of fit of some of the data, as discussed later in Section 4.1, three fits were performed for the six-aircraft dataset: (1) a conservative fit; here the two data sets across all wind conditions with the largest σ and ω values were the only ones considered by the fitting algorithm; (2) standard fit; all datasets were equally weighted as part of the fitting algorithm, as per the results presented in previous Sections and (3) optimistic fit; here the two data sets across all wind conditions with the smallest σ and ω values were the only ones considered by the fitting algorithm.

Figure 13 and Figure 14 show the translational heave and rotational pitch results for the six-aircraft dataset for the conservative curve fit turbulence model respectively. Figure 15 and Figure 16 show the corresponding results for the standard curve fit and Figure 17 and Figure 18 show the optimistic curve fit results.

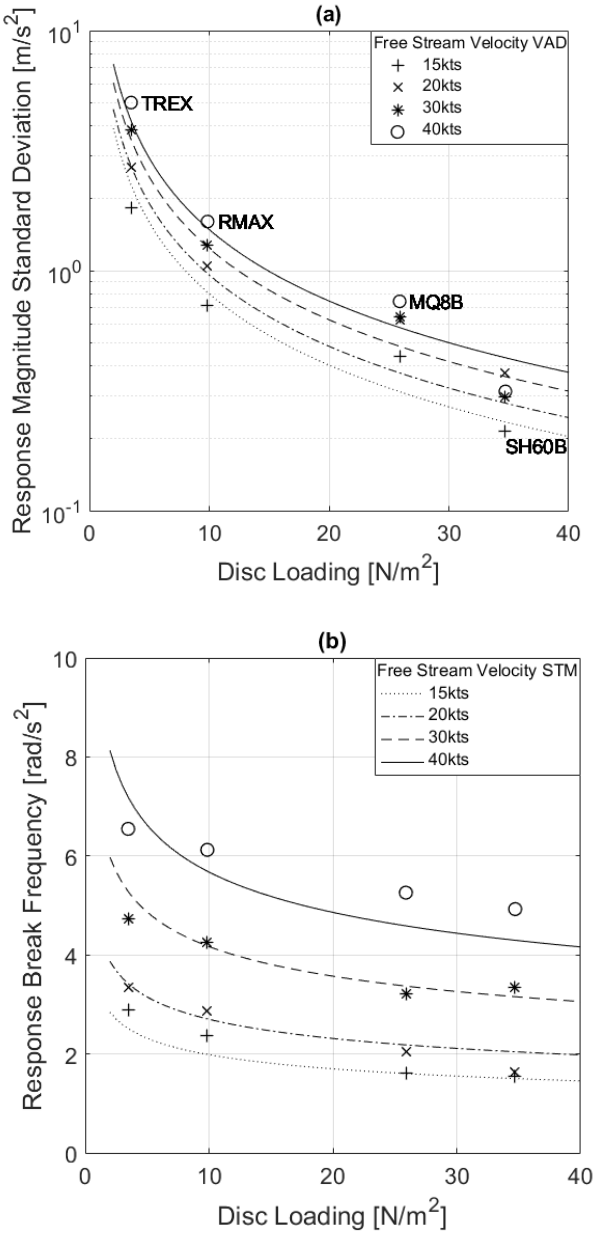

Figure 9. Turbulence model parameters based upon four aircraft model response datasets – translational heave axis

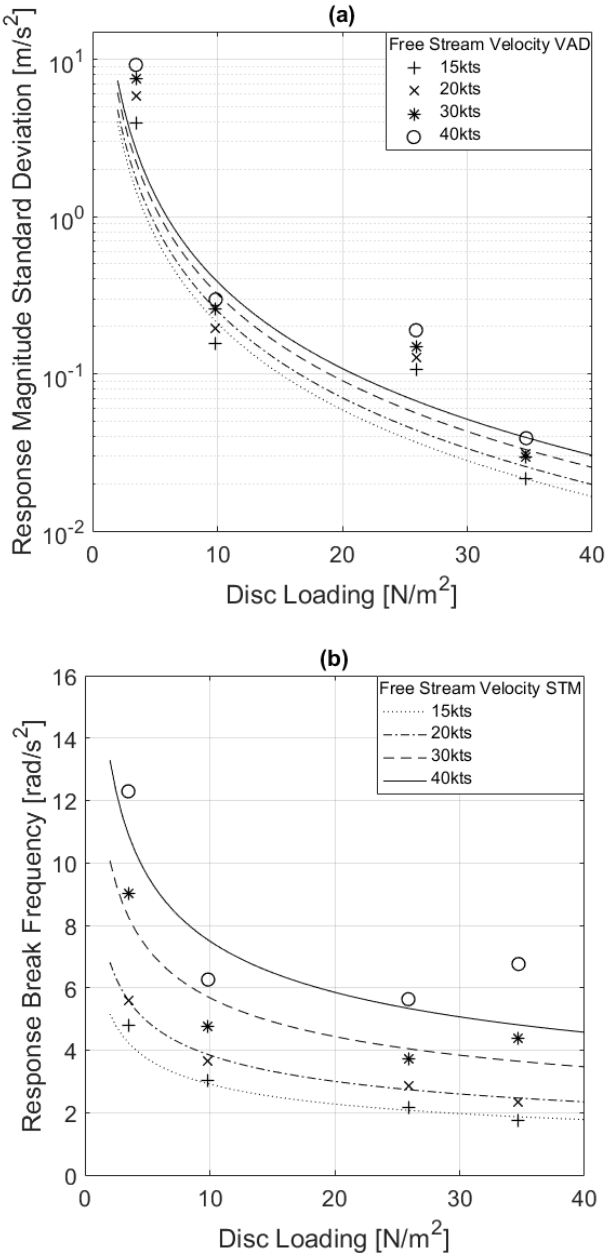

Figure 10. Turbulence model parameters based upon four aircraft model response datasets – rotational pitch axis

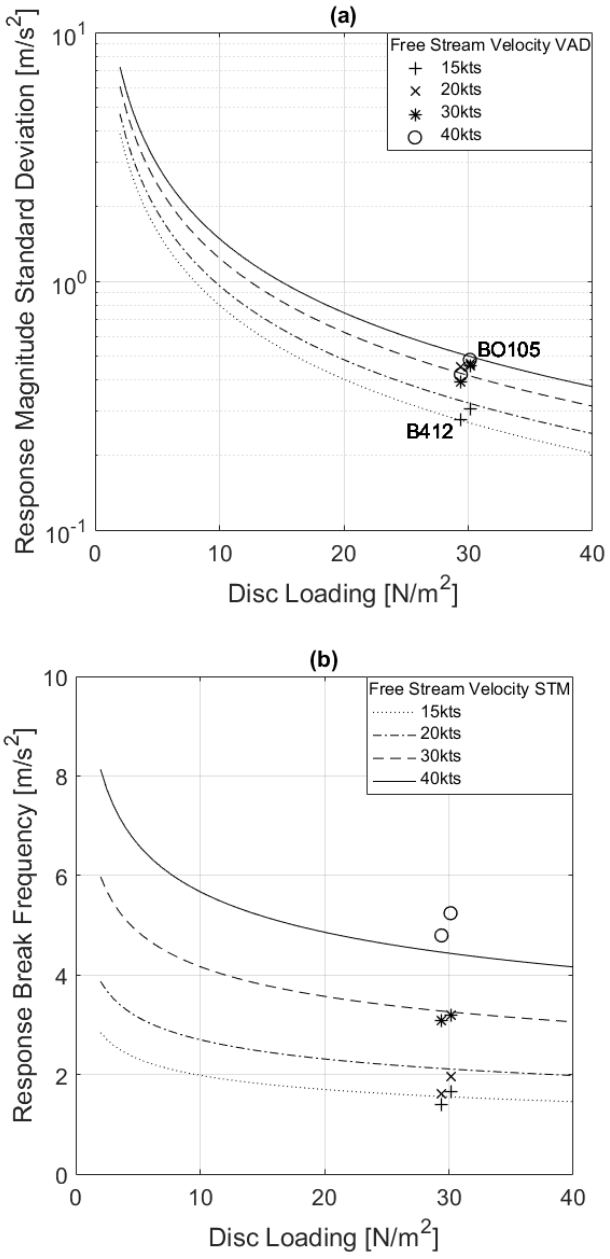

Figure 11. Comparison of unseen datasets with the turbulence model – translational heave axis

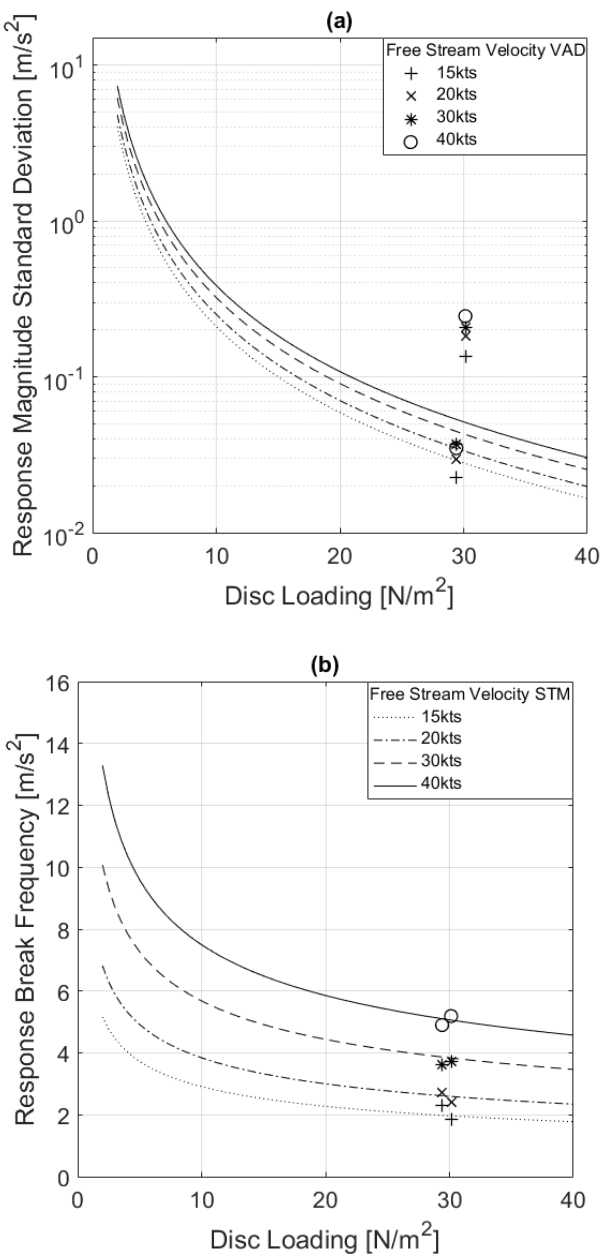

Figure 12. Comparison of unseen datasets with the turbulence model – rotational pitch axis

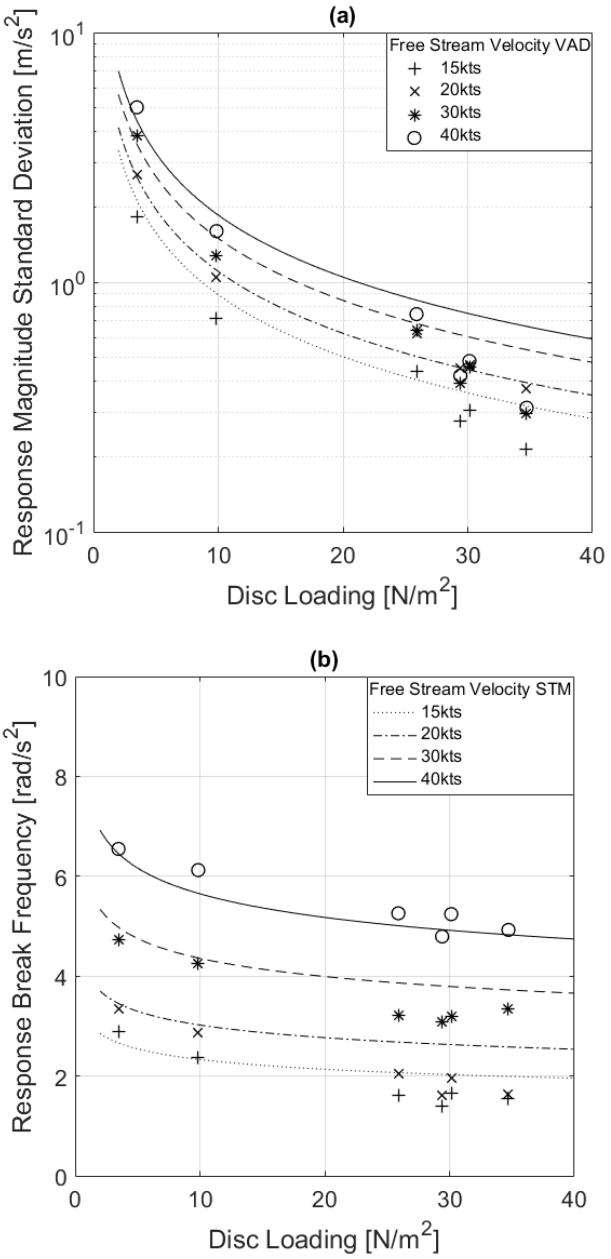

Figure 13. Translational heave axis turbulence model based upon six rotorcraft models – conservative fit

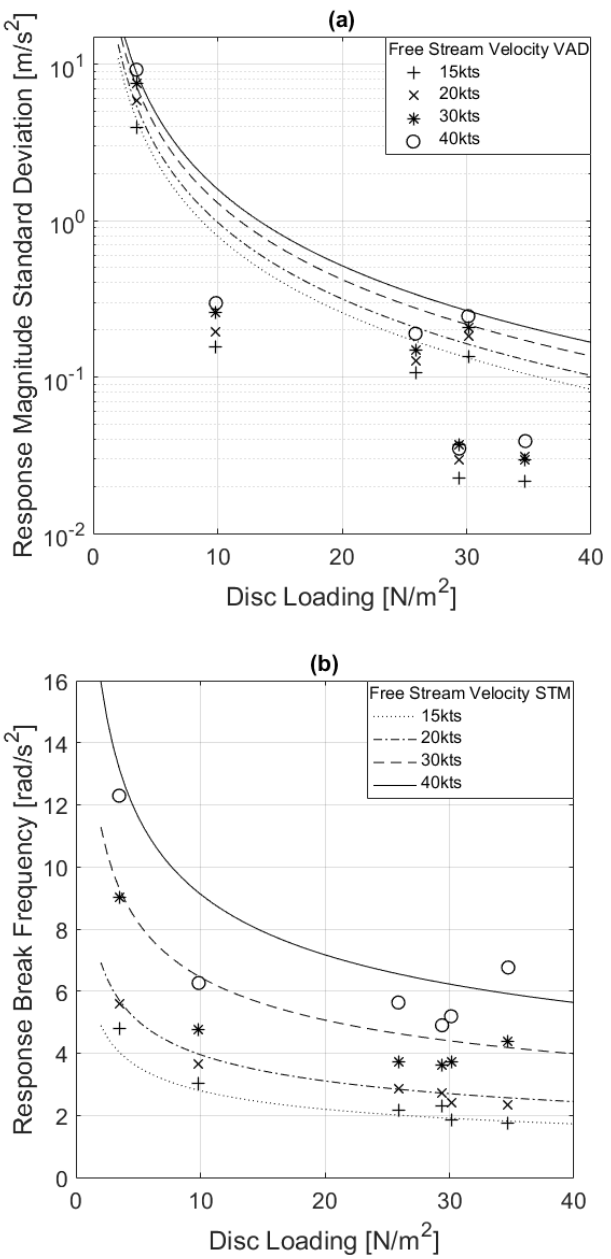

Figure 14. Rotational pitch axis turbulence model based upon six rotorcraft models – conservative fit

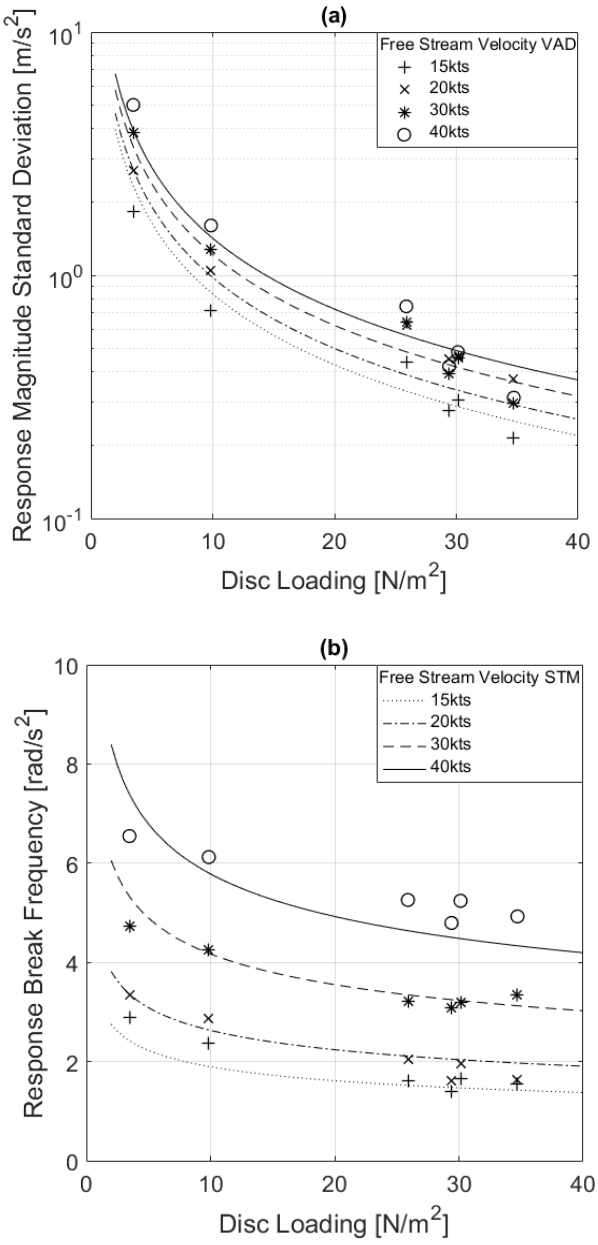

Figure 15. Translational heave axis turbulence model based upon six rotorcraft models – standard fit

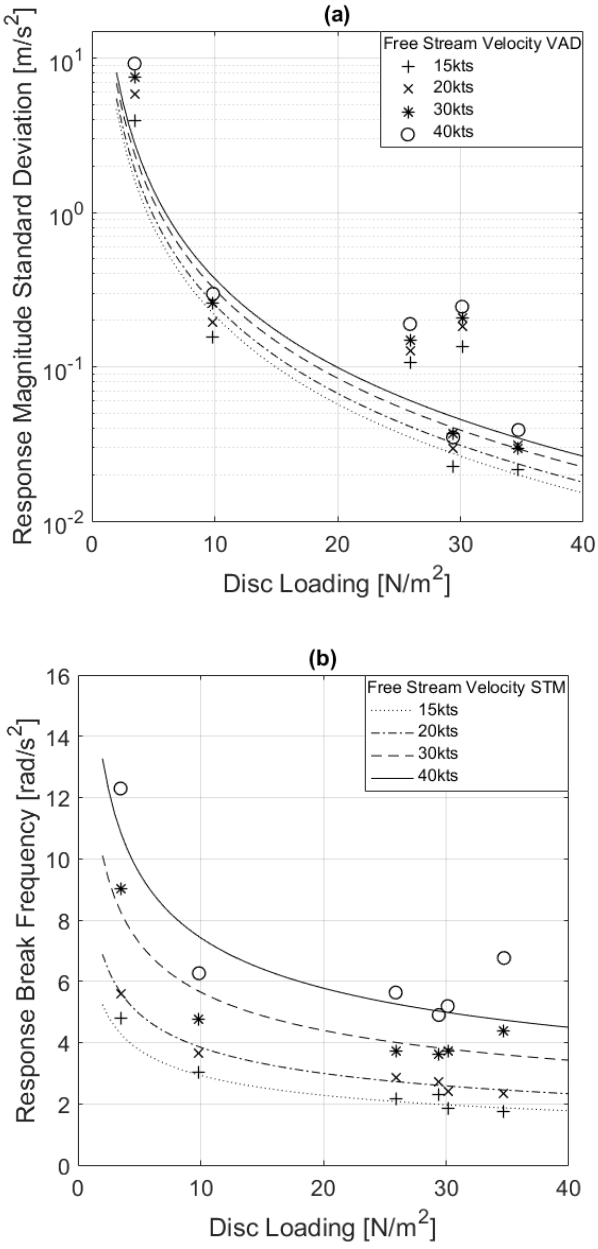

Figure 16. Rotational pitch axis turbulence model based upon six rotorcraft models – standard fit

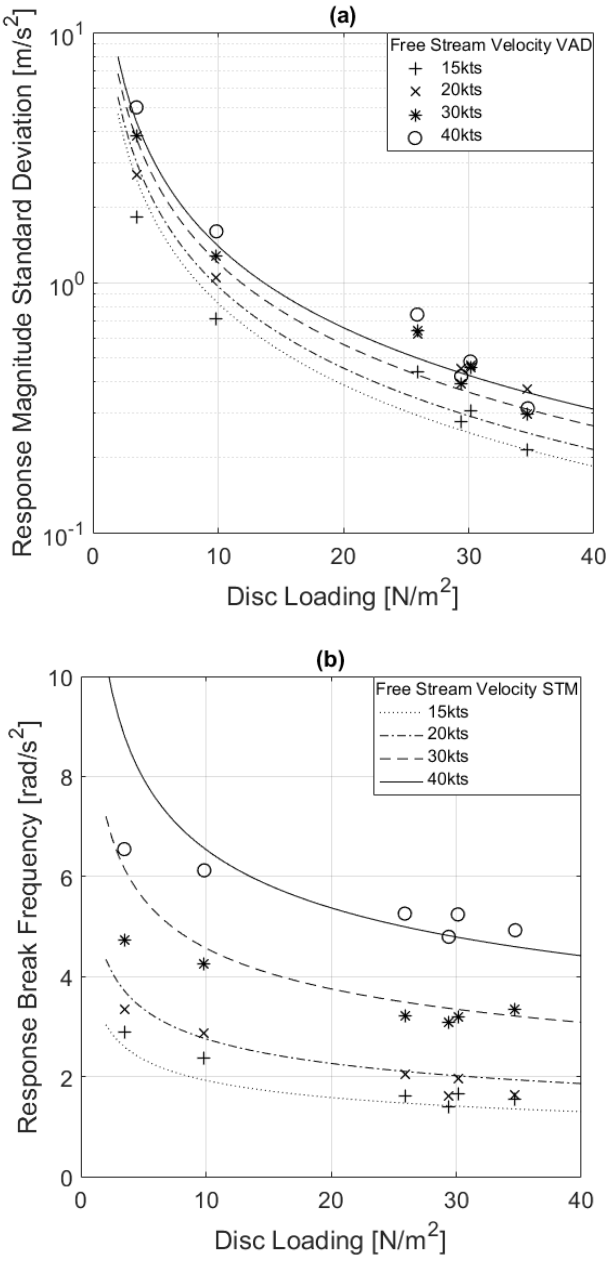

Figure 17. Translational heave axis turbulence model based upon six rotorcraft models – optimistic fit

4 DISCUSSION

4.1 Four Aircraft-based STM

By inspection, for the heave axis data of Figure 9(a), it can be seen that the process provides a reasonably good curve fit for the σ values but is somewhat non-conservative for the MQ8B data. It is also noted that the SH60B data points are non-monotonically increasing with wind speed – an implicit assumption of Eq. 3. For the corresponding break frequency data of Figure 9(b), they are well represented by the curve fit at the lower wind speeds but, at the highest wind speed, the curve fit is somewhat optimistic. For the The σ data is not well captured for the MQ8B and the break frequency data trend for the 30 and 40kt cases is less well captured than for the lower wind speeds. rotational axis data of Figure 10, the outcome is similar.

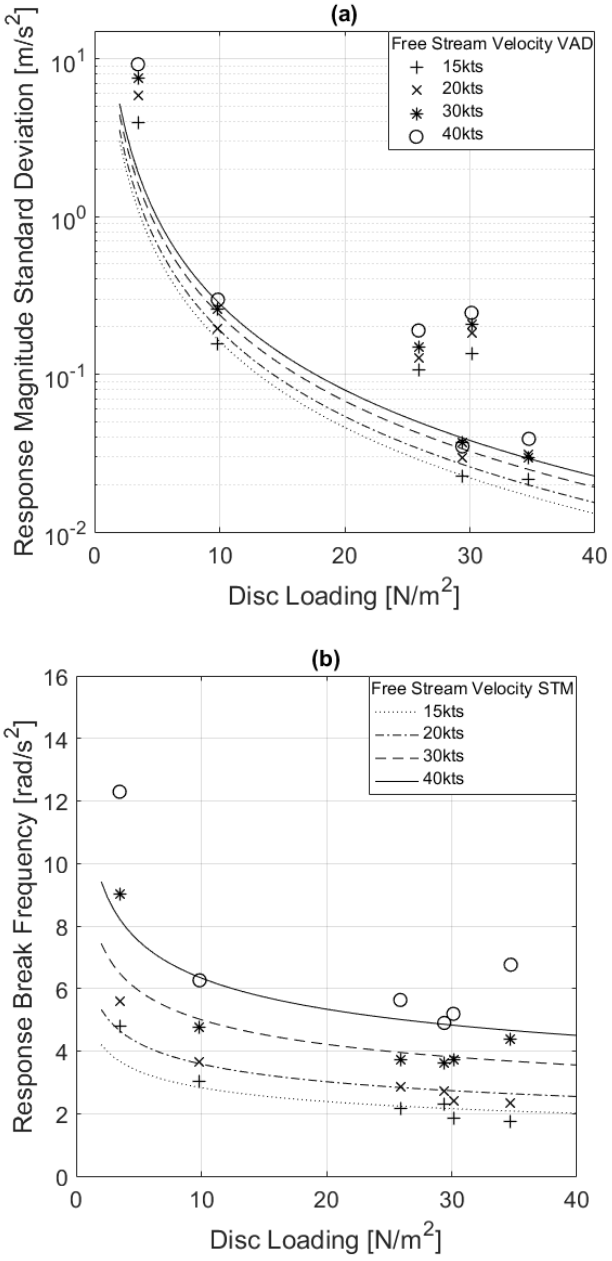

Figure 18. Rotational pitch axis turbulence model based upon six rotorcraft models – optimistic fit

4.2 Unseen Aircraft Comparison with the Four Aircraft-based STM

Considering the results of Figure 11, for the heave axis, it can be seen that the STM matches the σ and ω values well but is a little optimistic for the break frequencies for the 40kt case. For the rotational pitch axis, the STM curve fits provide a conservative prediction for the Bell 412HP model but are extremely optimistic for the BO105 model used. Although not shown in the paper, the rotational roll

response for the Bo105 was also not well captured by the STM model, as presented. The STM model provides a good prediction of the break frequency of the turbulent response for both aircraft.

4.3 Six Aircraft-based STM

For the conservative fit of the translational heave axis data of Figure 13, the STM provides a good estimate for σ at the lower disc loadings but becomes increasingly pessimistic as the disk loading increases. The same is true for the break frequency data except for the 40kt case where the STM is slightly optimistic, even for this conservative fit case. The reason that this can happen is that the fitting algorithm is trying to fit all of the data simultaneously to the model of Eqns. 3 and 4.

For the rotational pitch axis, shown in Figure 14, the σ data are now well predicted for the stiffer rotor models. The BO105 has quite a stiff hingeless rotor and is modelled as such. The TREX has a teetering rotor. The STM fit is now much less good for the other rotorcraft. The break frequencies are well modelled by the conservative fit for the lower wind speeds but less well for the higher wind speeds due to the larger scatter in the data.

Figure 15 is an updated version of Figure 9 but that now takes account of the additional two aircraft added into the overall dataset. The model captures the σ values reasonably well, although is somewhat optimistic for the 40kt wind case and for the MQ8B for all wind speeds. The break frequency data is well captured by the STM but is predicts lower frequency values at the higher disc loadings.

Similarly, Figure 16 shows an updated version of Figure 10, taking account of the six, rather than the 4 aircraft models. For this version of the fitting algorithm, the STM predicts the σ value reasonably well for the RMAX, Bell 412HP and SH60B aircraft but does less well for the other aircraft models. The break frequencies are well predicted for the lower wind speeds but, again, due to the larger scatter of results, the STM captures the trend less well for the higher wind speeds.

Comparing Figure 9 and Figure 17 for the translational heave axis, there is not a great deal of difference between the STM fitted curve results. The optimistic results produce curve data that with slightly reduced σ and ω predictions than their standard fit counterparts.

The STM model σ fits for the rotational pitch axis, shown in Figure 18(a), as would be expected given the method used, now show a good fit for the two datasets with the lowest prediction values, but optimistic results for the remaining aircraft model data. The break frequency data (Figure 18(b)) is still reasonably well modelled for the lower wind speeds, including the 30kt case for all but the lowest disc loading case. The STM is optimistic for the highest wind speed at high and low wind speeds.

4.4 Bringing it All Together

All of the data presented in this Section show that none of the curves fit the data perfectly; this is perhaps to be expected as the fitting routine is trying to fit the data monotonically increasing with wind speed. There are some cases where this is not the case e.g. the heave acceleration for the SH60B model, where the 20kt case produced the largest σ value. This is likely to be due to a localised effect of the flow conditions on the rotor but further analysis would be required to confirm this. It is worth noting of course that the σ plots show the standard deviation of the perturbations about the mean, and not the magnitude of the perturbation itself.

In general, for the models based upon a conventional articulated rotor, the standard deviation of the response magnitude from the mean (σ) seems to be well modelled by the standard fit curves. For rotorcraft with ‘stiffer’ rotors, this term seems to be better modelled by the conservative fit curves for the pitch axis (and the roll axis, but that data has not been presented in this paper). The standard fit curves appear to be satisfactory for the other states for this class of rotor head.

For the break frequency term of the presented STM (ω), the conservative fit curves appear to be the most suitable model for both types of rotor head investigated in this paper. Even here, the model is not always truly conservative but, in terms of predicting the vehicle perturbation, this term is the less important of the two.

4.5 Limitations

Whilst the work presented is this paper covers a wide range of helicopter MTOWs and disc loadings using methods validated in the literature, the work is based purely on modelling and simulation techniques. It would clearly be a significant task to validate the results presented with flight test data and this was well beyond the scope of the funded work. However, it would be of interest to be able to measure perturbations from flight test and determine how close to reality the predictions from the STM are.

It is acknowledged that the STM presented is only valid for conventional helicopter configurations, as these were the only types subject to the process. It is not known if the STM would change significantly for different vehicle configurations (e.g. multi-rotor) but, at this stage, the STM would not be recommended for use with ‘novel’ vertical lift configurations.

5 CONCLUDING REMARKS

This paper reports a process and toolset that has been created and used to generate a novel predictive method for the turbulence/perturbations that would be experienced by a rotorcraft in a ship air wake for each rigid body translational and rotational state. The derived scalable turbulence model consists of a transfer function whose standard deviation and break frequency relate to the ambient wind velocity and the rotor disc loading. 'Conservative', 'Standard' and 'Optimistic' version of the model have been created. For the standard deviation element of the model, the Standard version of the model appears to be the best fit, except for the pitch and roll axes of hingeless, stiffer rotor heads. The Standard model appears to be the best fit for all rotorcraft types for the break frequency term of the model.

ACKNOWLEDGEMENTS

The work reported in this paper was funded by the Defence Science and Technology Laboratory (Dstl) under contract DSTLX1000074725. The authors would like to thank the funder for the opportunity to conduct this work. The authors would also like to thank both the National Research Council of Canada for providing data and specifications for the T-REX helicopter model and DSTG in Australia for providing the RMAX model and their assistance for this study as part of The Technical Cooperation Program (TTCP).

REFERENCES

[1] Anon., "Helicopter/Ship Qualification Testing," RTO/NATO, RTO-AG-300 Vol. 22, 2003.

[2] Cox, I., Turner, G. and Finlay, B., "The ship/air interface framework (SAIF) project: Dynamic challenges", *RAeS Conference: Maritime Operations of Rotorcraft,* RAeS, London, UK, 11–12 June 2008.

[3] Hoencamp, A., White, M.D. and Perfect, P., "Proof of Concept for a Predictive Ship Helicopter Operational Limitation Analysis Tool", *37th European Rotorcraft Forum,* ERF, Gallarate, Italy, September 2011.

[4] Advani, S.K. and Wilkinson, C.H., "Dynamic interface modelling and simulation-a unique challenge", *Proceedings of the Royal Aeronautical Society conference on helicopter flight simulation,* RAeS, London, UK, November 2001.

[5] Scott, P. et al., "Using Piloted Simulation to Measure Pilot Workload of Landing a Helicopter on a Small Ship", *43rd European Rotorcraft Forum,* ERF, Milano. Italy, September 2017.

[6] Scott, P., White, M.D., and Owen, I., "The Effect of Ship Size on Airwake Aerodynamics and Maritime Helicopter Operations", *41st European Rotorcraft Forum,* ERF, Munich, Germany, September 2015.

[7] Kaaria, C. et al., "An experimental technique for evaluating the aerodynamic impact of ship superstructures on helicopter operations", *Ocean Engineering,* Vol. 61, 2013, pp. 97-108. 10.1016/j.oceaneng.2012.12.052

[8] Padfield, G.D. et al., "Predicting rotorcraft flying qualities through simulation modelling; a review of key results from *GARTEUR AG06*", *Proceedings of the 22nd European Rotorcraft Forum,* Brighton, U.K., 1996.

[9] Ockier, C.J., and von Grünhagen, W., "*BO 105 Flight Test Data Base for the Evaluation of ADS-33C Criteria*", DLR, DLR-Interner Bericht. 111-93/20, 53 S, Braunschweig, 1993.

[10] Perfect, P. et al., "A Rating Scale for the Subjective Assessment of Simulation Fidelity", *The Aeronautical Journal,* Vol. 11, No. 1206, 2014, pp. 953-974. 10.1017/S0001924000009635

[11] Perfect, P. et al., "Rotorcraft Simulation Fidelity: New Methods for Quantification and Assessment", *The Aeronautical Journal,* Vol. 117, No. 1189, 2013, pp. 235-282.

[12] Anon., "Strategic concept of employment for unmanned aircraft systems in NATO", The Joint Air Force Competence Centre, Kalkar, Germany, 2010.

[13] Forrest, J.S., and Owen, I., "An investigation of ship airwakes using Detached-Eddy Simulation", *Computers and Fluids,* Vol. 39, 2010, pp. 656-673. 10.1016/j.compfluid.2009.11.002

[14] Owen, I., White, M.D. and Padfield, G.D., "A Virtual Engineering Approach to the Ship-Helicopter Dynamic Interface; a decade of modelling and simulation research at The University of Liverpool", *The Aeronautical Journal,* Vol. 121, No. 1246, 2017, pp. 1833-1857.

[15] Kaaria, C.J., Forrest, J.S. and Owen, I., "The virtual AirDyn: a simulation technique for evaluating the aerodynamic impact of ship superstructures on helicopter operations", *The Aeronautical Journal,* Vol. 117, No. 1198, 2013, pp. 1233-1248.

[16] Tischler, M.B. and Remple, R.K., "Aircraft and Rotorcraft System Identification," American Institute of Aeronautics and Astronautics (Education Series), 2012.

[17] Hodge, S.J., Forrest, J.S. and Padfield, G.D., "Simulating the environment at the helicopter-ship dynamic interface: research, development & application", *The Aeronautical Journal,* Vol. 116, No. 1185, 2012, pp. 1155-1184.

APPENDIX

Table 1 contains the coefficients used in Equations 3 and 4 for the STM derived using six rotorcraft models.

Table 1. Scalable Turbulence Model Coefficients obtained using 6 Aircraft Models

		Aircraft Axis					
	Coefficient	**Surge**	**Sway**	**Heave**	**Roll**	**Pitch**	**Yaw**
Conservative Fit	a_σ	0.0404	0.0200	1.2901	11.2954	7.9660	0.0439
	b_σ	0.6923	0.9659	0.7482	0.7899	0.7050	1.5311
	c_σ	-0.4904	-0.3999	-0.8246	-1.6520	-1.6263	-1.0368
	a_ω	0.7631	0.7498	0.4921	1.7585	0.5288	0.6750
	b_ω	0.9270	0.9197	0.9030	0.9302	1.2064	0.9215
	c_ω	-0.3053	-0.2203	-0.1260	-0.4194	-0.3477	-0.0998
Standard Fit	a_σ	0.0505	0.0175	2.5937	13.3673	5.6168	0.1058
	b_σ	0.6577	1.0373	0.5370	0.5398	0.5591	1.2002
	c_σ	-0.6086	-0.4646	-0.9673	-1.9404	-1.9122	-1.0784
	a_ω	0.6871	0.6597	0.3163	0.7157	0.9683	0.6593
	b_ω	1.0088	0.9769	1.1373	1.0103	0.9484	0.9081
	c_ω	-0.3750	-0.2334	-0.2317	-0.2508	-0.3612	-0.0856
Optimistic Fit	a_σ	0.0907	0.0199	3.3410	8.8660	3.3889	0.2750
	b_σ	0.7786	1.0562	0.5370	0.5498	0.5572	1.1361
	c_σ	-0.9677	-0.5724	-1.0835	-1.9008	-1.8152	-1.3791
	a_ω	0.9383	0.5972	0.2887	0.6764	0.9306	0.7637
	b_ω	0.9367	1.0285	1.2473	0.9983	0.8221	0.8399
	c_ω	-0.4404	-0.2514	-0.2831	-0.2611	-0.2467	-0.0685

Table 2 contains the coefficients used in Equations 3 and 4 for the STM derived using four rotorcraft models.

Table 2. Scalable Turbulence Model Coefficients obtained using 4 Aircraft Models

	Aircraft Axis					
Coeff	**Surge**	**Sway**	**Heave**	**Roll**	**Pitch**	**Yaw**
a_σ	0.0380	0.0200	1.2900	13.4066	11.0089	0.0439
b_σ	0.7677	0.9659	0.7482	0.8340	0.7114	1.5311
c_σ	-0.5846	-0.3999	-0.8246	-1.8748	-1.8987	-1.0368
a_ω	0.7632	0.7664	0.4920	1.9151	0.5288	0.6749
b_ω	0.9270	0.8957	0.9030	0.8855	1.2064	0.9215
c_ω	-0.3052	-0.1883	-0.1260	-0.4064	-0.3476	-0.0998
a_σ	0.0447	0.0161	2.1583	7.9990	4.0499	0.0782
b_σ	0.7586	1.0486	0.6275	0.5505	0.6174	1.3789
c_σ	-0.6828	-0.4318	-0.9874	-1.7269	-1.8329	-1.1607
a_ω	0.8329	0.6738	0.3715	0.7654	0.9211	0.7092
b_ω	0.9329	0.9638	1.0716	0.9804	0.9643	0.8764
c_ω	-0.3801	-0.2256	-0.2235	-0.2416	-0.3561	-0.0802
a_σ	0.0907	0.0119	3.3409	3.6710	1.8930	0.2750
b_σ	0.7786	1.0766	0.5370	0.5305	0.5946	1.1361
c_σ	-0.9677	-0.3720	-1.0835	-1.4944	-1.6016	-1.3791
a_ω	0.9385	0.5972	0.2889	0.6764	0.9305	0.7637
b_ω	0.9367	1.0284	1.2473	0.9983	0.8221	0.8399
c_ω	-0.4404	-0.2514	-0.2833	-0.2611	-0.2467	-0.0685